Spatiotemporal Atlas Estimation for Developmental Delay Detection in Longitudinal Datasets

Stanley Durrleman, Xavier Pennec, Guido Gerig, Alain Trouvé, Nicholas Ayache

INSTITUT NATIONAL DE RECHERCHE EN INFORMATIQUE ET EN AUTOMATIQUE

Spatiotemporal Atlas Estimation for Developmental Delay Detection in Longitudinal Datasets

Stanley Durrleman — Xavier Pennec — Guido Gerig — Alain Trouvé — Nicholas Ayache

N° 6952

June 2009

Thème BIO

ISSN 0249-6399 ISRN INRIA/RR--6952--FR+ENG

Spatiotemporal Atlas Estimation for Developmental Delay Detection in Longitudinal Datasets

Stanley Durrleman[*] [†] , Xavier Pennec[*] , Guido Gerig[‡] , Alain Trouvé[†] , Nicholas Ayache[*]

Thème BIO — Systèmes biologiques
Projet Asclepios

Rapport de recherche n° 6952 — June 2009 — 17 pages

Abstract: We propose a new methodology to analyze the anatomical variability of a set of longitudinal data (population scanned at several ages). This method accounts not only for the usual 3D anatomical variability (geometry of structures), but also for possible changes in the dynamics of evolution of the structures. It does not require that subjects are scanned the same number of times or at the same ages. First a regression model infers a continuous evolution of shapes from a set of observations of the same subject. Second, spatiotemporal registrations deform jointly (1) the geometry of the evolving structure via 3D deformations and (2) the dynamics of evolution via time change functions. Third, we infer from a set of subjects a prototype scenario of evolution and its 4D variability within the population. Our method is used to analyze the morphological evolution of 2D profiles of hominids skulls and to analyze brain growth from amygdala of autistics, developmental delay and control children.

Key-words: Computational Anatomy , longitudinal data , spatiotemporal variability , 4D registration , time regression , atlas construction , large deformation , diffeomorphism , currents

[*] Asclepios team project, INRIA Sophia Antipolis, France
[†] Centre de Mathématiques et Leurs Applications (CMLA), ENS-Cachan, France
[‡] Scientific Computing and Imaging Institute, University of Utah

Unité de recherche INRIA Sophia Antipolis
2004, route des Lucioles, BP 93, 06902 Sophia Antipolis Cedex (France)
Téléphone : +33 4 92 38 77 77 — Télécopie : +33 4 92 38 77 65

Estimation d'atlas spatio-temporels pour la détection de retards de dévelopement à partir de données longitudinales

Résumé : Nous proposons une nouvelle méthodologie pour l'analyse de la variabilité anatomique d'un ensemble de données longitudinales (un ensemble de sujets observés à plusieurs instants). Cette méthode ne prend pas seulement en compte la variabilité anatomique 3D usuelle (la géométrie des structures), mais aussi de possibles changements dans la dynamique d'évolution de ces structures. Les sujets n'ont pas besoin d'être observés le même nombre de fois, ni aux mêmes âges. Tout d'abord, un modèle de régression déduit d'un ensemble d'observations d'un même sujet une évolution continue de forme. Ensuite, des recalages spatio-temporels déforment conjointement (1) la géométrie de la structure en évolution grâce à des déformations 3D et (2) la dynamique d'évolution grâce à des fonctions de changement de temps. Enfin, on déduit d'un ensemble de sujets un scenario prototype d'évolution ainsi que sa variabilité 4D au sein de la population. Notre méthode est utilisée pour l'analyse de l'évolution morphologique de profils 2D de crânes d'hominidés et pour l'analyse de la croissance des amygdales chez des enfants autistes, attardés mentaux et sains.

Mots-clés : Anatomie numérique , données longitudinales , variabilité spatio-temporelle , recalage 4D , régression temporelle , construction d'atlas , grande déformation , diffeomorphisme , courant

1 Methodology for Statistics on Longitudinal Data

Many frameworks has been already proposed in medical imaging to analyze the anatomical variability of 3D structures like images, curves or surfaces. Less attention has been paid to the variability of longitudinal data (several subjects scanned several times). In [1], the evolution between two shapes is modeled by a geodesic deformation, which cannot be used for more than two data per subjects. In [2], shape growth is measured via the evolution of extracted features like volumes, shape or pose parameters. In [3, 4, 5], a temporal regression is proposed globally for a population or for one sequence of observations: this does not allow inter-subject comparisons (i.e. comparison between two sequences acquired for two different subjects). In cardiac motion analysis [6, 7], spatiotemporal registration relies on 3D-registrations between images of the same moment of the cardiac cycle and between two consecutive time-points. These works rely on time-point correspondence and do not call the labels of the time-points into question. By contrast, in longitudinal studies, subjects are scanned at ages which do not necessarily correspond. Moreover, evolutions may be delayed or advanced within a population, a key feature that we precisely aim at detecting. In [8, 9], deformation of cardiac motion are proposed both in space and time but they require a fine temporal sampling of the motion, whereas only few acquisitions per subjects are available in most longitudinal studies. In this report, we propose to use a regression model to estimate a continuous evolution from data sparsely distributed in time and spatiotemporal deformations which register jointly both the 3D geometry and the scenario of evolution of two different subjects. Geometrical data are modeled as currents to avoid assuming point correspondence between geometrical structures. Large deformations are used which gives a rigorous framework for statistics on deformations and atlas construction [10, 11, 12]. From longitudinal data, we estimate consistently the most likely scenario of evolution and its spatiotemporal variability within the population.

In this report, we call longitudinal data a set of geometrical data (curves or surfaces, called here shapes), acquired from different subjects scanned at several time-points. We assume that the successive data of a given subject are temporal samples of a continuous evolution. We propose therefore a **regression model** which computes a continuous evolution which matches the data of the subject at the corresponding time points (Fig. 1). This continuous evolution allows us to compare two subjects at a given age, even if one subject has not been scanned at this age. We can also analyze how the shape varies near this age to detect possible developmental delays. We define then the **spatiotemporal deformation** of a continuous evolution, which consists of two deformations: (1) a morphological deformation (of the 3D space) which changes the geometry of every frame of the evolution *independently of the time point* and (2) a time change function (deformation of the time interval) which changes the dynamics of the evolution *without changing the geometry of shapes*. To avoid time-reversal, the time change function must be smooth and order preserving: it is a diffeomorphism of the time interval of interest. A **4D registration** between two subjects looks for the most regular spatiotemporal deformation, such that the deformation of the continuous evolution inferred from the first subject maps the successive target data (Fig. 2). Eventually, we use this 4D registration framework to estimate a **spatiotemporal atlas** from a population, based on an 4D extension of the statistical model of [12]. We look for a template and a continuous evolution of this template (called mean scenario of evolution), so that data of each subject are temporal samples

of a spatiotemporal deformation of the mean scenario. A Maximum A Posteriori estimation enables to estimate consistently the template, the mean scenario and the spatiotemporal deformations of this mean scenario to each subject.

We present the regression framework in Section 2, the 4D-registration scheme in Section 3 and the atlas construction in Section 4. In Section 5, we present spatiotemporal registrations of 2D profiles of hominids skulls and atlas estimation from a set of amygdala of autistics, developmental delay and control children, scanned at age 2 and 4 years.

2 Regression Model for Shape Evolution

We want to fit a continuous shape evolution to a set of shapes (S_i) of the same subject acquired at different time points (t_i). Without loss of generality, we can assume that $t_{\min} = 0$ and $t_{\max} = T$. This evolving shape is equal to the baseline M_0 at time $t = 0$, which may be the earliest shape of this subject or a template as in Sec. 4. The evolution has the form: $M_t = \chi_t(M_0)$ where t varies continuously in the time interval $[0, T]$. For each t, χ_t is a diffeomorphism of the 3D space, such that $\chi_0 = \mathrm{Id}$ (which leads to $\chi_0(M_0) = M_0$). The regression (M_t) must match the observations S_i at the time-points t_i, while a rigidity constraint controls the regularity of the regression. This is achieved by minimizing:

$$J(\chi) = \sum_{t_i} \mathrm{d}(\chi_{t_i}(M_0), S_i)^2 + \gamma^{\chi} \mathrm{Reg}(\chi) \tag{1}$$

where d is a similarity measure between shapes, $\mathrm{Reg}(\chi)$ a regularity term and γ^{χ} a trade-off between regularity and fidelity to data. Among other possible choices, we use here the large deformations of [13], and model curves or surfaces as currents [14, 11]. Therefore, d is the distance between currents and χ is the solution of the flow equation :

$$\frac{\partial \chi_t(x)}{\partial t} = v_t^{\chi}(\chi_t(x)) \tag{2}$$

with initial condition $\chi_0 = \mathrm{Id}$. At every time t, v_t is the speed vector field in the Eulerian coordinates, which gives the speed of a particle which flows by the fixed position x at time t. The regularity term $\mathrm{Reg}(\chi)$ is given by the total kinetic energy of the deformation: $\int_0^T \|v_t^{\chi}\|_V^2 \, dt$ (for a norm on the space of speed vector field V, still to be defined).

If there were only one data S_1 at time $t_1 = T$, this would be exactly the registration of M_0 to S_1, as stated and solved in [14, 15, 16]. The result is a geodesic flow of diffeomorphism between $t = 0$ and $t = T$ that maps M_0 closely to S_1. With several data at successive time points, the result is a flow of diffeomorphism which geodesic only between successive time points (i.e. piecewise geodesic).

In this report, we deal with point-based data (set of unconnected points, curves or surfaces, but not continuous images for instance). In this case, we enforce also the speed vector field v_t^{χ} to belong to a reproducible kernel Hilbert space (r.k.h.s.) with kernel K^{χ}, so that the time-varying vector field v^{χ} which minimizes the criterion J results from an interpolation in the Hilbert space V [17, 16]:

$v_t^\chi(x) = \sum_{p=1}^N K^\chi(x, x_p(t))\alpha_p(t)$, where the x_p are the N points of the source data M_0, $x_p(t)$ their trajectory in the 3D space ($x_p(t) = \chi_t(x_p)$), and α_p a discrete set of moving momenta (3D vectors). The Hilbert norm of v_t^χ for a fixed t is given by: $\|v_t^\chi\|_V^2 = \sum_{p,q=1}^N \alpha_p(t)^T K^\chi(x_p(t), x_q(t))\alpha_q(t)$. The moving points of M_0 ($\chi_t(M_0)$) are solution of the integral equation (integrating the flow equation Eq. (2)): $x_p(t) = x_p + \int_0^t K^\chi(x_p(u), x_q(u))\alpha_q(u)du$. The positions of the moving M_0 depend therefore only on the momenta $\alpha_p(t)$. As a consequence, all terms in the criterion J depend only on the variables $\alpha_p(t)$, which are used for the gradient descent. As shown in the appendix, the gradient of J (as a mapping from N square integrable functions α_p to $\mathbb{R}$) is given by:

$$(\nabla J)_p(t) = 2\gamma^\chi \alpha_p(t) + \eta_p(t) \tag{3}$$

where $\eta_p(t)$ is the solution of the integral equation for all p:

$$\begin{aligned}\eta_p(t) = &\sum_{t_i} \nabla_{x_p(t_i)} A_i \mathbf{1}_{\{t \le t_i\}} \\ &+ \int_t^T \left(\sum_q (\partial_1 + \partial_2)(K^\chi(x_p(u), x_q(u))\alpha_q(u)) \right)^T (\gamma^\chi \alpha_p(u) + \eta_p(u))du\end{aligned} \tag{4}$$

where $A_i = \mathrm{d}(\chi_{t_i}(M_0), S_i)^2$ and ∂_i denotes the derivative with respect to the i-th variable and $\mathbf{1}_{\{t \le t_i\}} = 1$ if $t \le t_i$ and 0 otherwise. Since d is here the distance in the space of currents, the gradient of A_i with respect to the points position $x_p(t_i)$ is computed as in [14, 16]. In our computations, we choose K^χ a isotropic Gaussian kernel: $K^\chi(x, y) = \exp(|x - y|^2 / \lambda_\chi^2)$. The standard deviation λ_χ determines the rigidity of the interpolation which leads to the speed vector field v^χ. It is therefore a spatial scale under which the motions of two points in the space are highly correlated.

We start the gradient descent by setting $\alpha_p(t) = 0$ for all t and p ($\chi_t = \mathrm{Id}$, for all t). The integration of the flow equation (Eq. (2)) and the Eq. (4) are performed by a centered Euler scheme, once the time interval is divided into N_{time} time steps. The integration of Eq. (4) is performed upstream in time. The initial conditions at $t = T$ is given by $\nabla_{x_p(T)} A_T$. Then the ODE is integrated for decreasing time t. As soon as a new time point t_i is reached, a new contribution $\nabla_{x_p(t_i)} A_i$ is added to η_u. As a consequence, $(\nabla J)_p(t)$ (and therefore the momenta $\alpha_p(t)$ and the vector field v_t^χ) at time t depend on all the data which appear later than t. Once the vector field is updated, the new positions $x_p(t)$ are computed by the integration of the flow equation Eq. (2) downstream in time (the initial condition is given at time $t = 0$ by $x_p(0) = x_p$). These positions at time t depend on the vector field v_t^χ for all time earlier than t. As a result, the positions $x_p(t)$ depend on all the data in past and future. This regression fits the best trajectory ($\chi_t(M_0)$) to all the data *globally*. This differs, for instance, from pairwise registrations between consecutive time-points, although both techniques result in a piecewise geodesic flow.

The function χ can be extended at all times by assuming $v_t^\chi = 0$ (and hence χ_t constant) outside the time interval $[0, T]$. This is a useful property in order to compare this evolution with new observations which may correspond to a time point outside this interval.

3 Spatiotemporal Pairwise Registration

We assume now that we have successive shapes for the source subject $(S(t_i))_i$ and for the target $(T(t_j))_j$. As in Sec. 2, we perform a regression on the source shapes which leads to a continuous evolution $S(t)_{t\in[0,T]}$, extended by constant mappings to an evolution $S(t)$ for every time t. Our goal is to find a diffeomorphism of the 3D space ϕ and a diffeomorphism of the time-interval ψ which deform the source evolution $S(t)$ into $S'(t) = \phi(S(\psi(t)))$ such that $S'(t_j)$ match $T(t_j)$. Thanks to the regression function, no correspondence is needed between the time points t_i and t_j. Formally, we minimize:

$$J(\phi,\psi) = \sum_{t_j} \mathrm{d}(\phi(S(\psi(t_j))), T_{t_j})^2 + \gamma^{\phi}\mathrm{Reg}(\phi) + \gamma^{\psi}\mathrm{Reg}(\psi) \tag{5}$$

The spatial deformation ϕ and the temporal deformation ψ are solution at parameter $u = 1$ of the flow equations[1]:

$$\frac{\partial\phi_u(x)}{\partial u} = v_u^{\phi}(\phi_u(x)) \quad \frac{\partial_u\psi_u(t)}{\partial u} = v_u^{\psi}(\psi(t)) \tag{6}$$

Like in the previous section, we enforce v_u^{ϕ} (resp. v_u^{ψ}) to belong to a r.k.h.s with kernel K^{ϕ} (resp. K^{ψ}). The source trajectory $S(t)$ is therefore described by the points $x_{p,t}$, where p denotes the index of the points of S, and t a time within the continuous interval ($t \in [0,T]$). In the matching term, the deformation ϕ_u is applied to the points $x_{p,\psi_1(t_j)}$ for all points p and time points t_j. The same arguments as in the previous section and in [17, 14] lead to the parameterization of the minimizing velocity field v_u^{ϕ} with momenta $\alpha_{p,j}(u)$ at the points $x_{p,\psi_1(t_j)}(u)$:

$$v_u^{\phi}(x) = \sum_{p,t_j} K^{\phi}(x, x_{p,\psi_1(t_j)}(u))\alpha_{p,j}(u) \tag{7}$$

Similarly, v_u^{ψ} is parametrized by the momenta $\beta_j(u)$ at time points $t_j(u)$:

$$v_u^{\psi}(t) = \sum_{j} K^{\psi}(t, t_j(u))\beta_j(u) \tag{8}$$

In the previous equations, $x_{p,t_j}(u) = \phi_u(x_{p,t_j})$ and $t_j(u) = \psi_u(t_j)$. The regularity parameters are defined by: $\mathrm{Reg}(\phi) = \int_0^1 \sum_{k,j,k',j'} \alpha_{p,j}(u)^T K^{\phi}(x_{p,\psi_1(t_j)}(u), x_{p',\psi_1(t_{j'})}(u))\alpha_{p',j'}(u)du$ and $\mathrm{Reg}(\psi) = \int_0^1 \sum_{j,j'} \beta_j(u)^T K^{\psi}(t_j(u), t_{j'}(u))\beta_{j'}(u)du$.

3.1 Exact derivation of the criterion

The criterion J depends on the L^2 functions $\alpha_{p,j}(u)$ and $\beta_j(u)$. The derivation of J with respect to the spatial momenta α is performed as for a 3D registration (this is a particular case of the derivation

[1] In the sequel, we may write therefore ϕ and ψ instead of ϕ_1 and ψ_1

made in the appendix with constraints only at the final parameter $u = 1$. Here the deformation parameter u plays the role of t in the appendix). This leads to the following gradient:

$$\nabla_{\alpha_{p,j}(u)} J(u) = 2\gamma^{\phi}\alpha_{p,j}(u) + \eta^{\phi}_{p,j}(u) \tag{9}$$

with $\eta^{\phi}_{p,j}(u)$ solution of the integral equation:

$$\begin{aligned}\eta^{\phi}_{p,j}(u) =& \nabla_{\phi_1(x_{p,t_j(1)})} A \\ &+ \int_u^1 \sum_{p',t'_j} \Big((\partial_1 + \partial_2)K^{\phi}(x_{p,t_j(1)}(s), x_{p',t'_j(1)}(s))\alpha_{p',j'}(s)\Big)^T (\gamma^{\phi}\alpha_{p,j}(s) + \eta^{\phi}_{p,j}(s))ds\end{aligned} \tag{10}$$

where A is the fidelity-to-data term $A = \sum_{t_j} \mathrm{d}(\phi(S(\psi(t_j))), T_{t_j})^2$. Its derivation with respect to the spatial positions $\phi_1(x_{p,t_j(1)})$ when the distance d is the distance in the space of currents is performed as in [14, 16].

The derivation of J with respect to the temporal momenta β is slightly more complex, since the spatial velocity field v^{ϕ}_u depends on the deformation ψ, as shown in Eq. (7). However, the term $\mathrm{Reg}(\phi) = \int_0^1 \left\|v^{\phi}_u\right\|^2 du$ depends on ψ only via the time $\psi_1(t_j)$ at the final parameter $u = 1$ (and not via the intermediate time points $\psi_u(t_j)$). It can be considered therefore as part of an extended fidelity term, which is of the form $\tilde{A}(\psi_1(t_1), \ldots, \psi_1(t_n)) = \sum_{t_k} \mathrm{d}(\phi(S(t_k(1))), T_{t_k})^2 + \gamma^{\phi} \int_0^1 \left\|v^{\phi}_u\right\|^2 du$. The derivation is performed now like in the appendix, but limited to a 1D domain. This leads to the following gradient:

$$\nabla_{\beta_j} J(u) = 2\gamma^{\psi}\beta_j(u) + \eta^{\psi}_j(u) \tag{11}$$

where $\eta^{\psi}_j(u)$ is the solution of the integral equation:

$$\eta^{\psi}_j(u) = \frac{\partial \tilde{A}}{\partial t_j(1)} + \int_u^1 \sum_{j'} \left((\partial_1 + \partial_2)K^{\psi}(t_j(s), t_{j'}(s))\beta_{j'}(s)\right)^T (\gamma^{\psi}\beta_j(s) + \eta^{\psi}_j(s))ds \tag{12}$$

The derivation of the fidelity-to-data term (first term in $\tilde{A}$) with respect to the temporal points $t_j(1)$ is of the form $\partial \left\|\phi(S(t)) - T\right\|^2 / \partial t$. It is approximated by a centered Euler scheme: $\sim \langle \phi(S(t)) - T, \phi(S(t+\delta t)) - \phi(S(t-\delta t))\rangle / \delta t$ (although an exact computation would have been possible, but at a high computational cost). We used here the fact that the shapes are embedded with a vector space (the space of currents) provided with an inner product. Now, we must derive the regularity term $\int_0^1 \left\|v^{\phi}_u\right\|^2 du$ with respect to the variables $t_j(1) = \psi_1(t_j)$. We have:

$$\begin{aligned}&\frac{\partial}{\partial t_j(1)} \alpha_{p,j}(u)^T K^{\phi}(x_{p,t_j(1)}(u), x_{q,t_k(1)}(u))\alpha_{q,k}(u) = \\ &2h'\left(\left\|x_{p,t_j(1)}(u) - x_{q,t_k(1)}(u)\right\|^2\right) \alpha_{p,j}(u)^T \alpha_{q,k}(u)(x_{p,t_j(1)}(u) - x_{q,t_k(1)}(u))^T \frac{\partial x_{p,t_j(1)}(u)}{\partial t_j(1)}\end{aligned} \tag{13}$$

when the kernel K^ϕ is a scalar kernel of the form: $K^\phi(x,y) = h(\|x-y\|^2)\mathrm{I}_3$ (for a given scalar function h like a Gaussian function for instance). This leads to the derivation:

$$\frac{\partial \int_0^1 \left\|v_u^\phi\right\|^2 du}{\partial t_j(1)} = 4\int_0^1 \sum_{p,q,i} h'\left(\left\|x_{p,t_i(1)}(u) - x_{q,t_j(1)}(u)\right\|^2\right) \alpha_{p,i}(u)^T \alpha_{q,j}(u)(x_{q,t_j(1)}(u) - x_{p,t_i(1)}(u))^T \frac{\partial x_{q,t_j(1)}(u)}{\partial t_j(1)} du \tag{14}$$

Since $x_{p,t_j(1)}(u) = \phi_u(x_{p,t_j(1)})$, the last term is equal to $\partial x_{p,t_j(1)}(u)/\partial t_j(1) = d_{x_{p,t_j(1)}}\phi_u\left(v^\chi_{t_j(1)}\right)$. If we do not keep track of the velocity field v^χ that generated the source evolution $S(t)$, or if we want to avoid the computation of the Jacobian matrix of ϕ_u, this term may be approximated with a centered Euler scheme: $\partial x_{p,t_j(1)}(u)/\partial t_j(1) \sim (x_{p,t_j(1)+\delta t} - x_{p,t_j(1)-\delta t})/(2\delta t)$.

The integration over the parameter $u \in [0,1]$ are performed by a centered Euler scheme, once the interval $[0,1]$ has been divided into N_u time steps. We discretize temporal evolutions of points by dividing the time interval $[0,T]$ into N_{time} time-steps.

Note that since the growth model χ_t is piecewise geodesic, the evolution $S(t)$ generated by χ_t is not differentiable at points t_j ($S(t)$ may have different left and right derivatives: $v^\chi_{t_j}$ is discontinuous at these points). This is an issue mainly during the first step of the gradient descent, since then $\psi = \mathrm{Id}$. Otherwise, one needs to derive $S(t)$ only at time-points $\psi_u(t_j)$ which have little chance to be one of the $\{t_j\}$. In practice, the derivation of $S(t)$ at t_j is made via a centered Euler scheme, which implicitly smoothes the vector field v^χ_u by averaging the left and right values at points t_j.

Note that we minimize J with respect to the geometrical and the temporal parameters *jointly*. We do not performed alternated minimization.

3.2 A suboptimal approach

The gradient of the criterion J involves the derivation of $\mathrm{Reg}(\phi)$ with respect to the temporal parameter β as computed in Eq. (14). This term is a coupling between temporal and geometrical parameters and can be seen as a correction of the derivative of the fidelity-to-data term. However, this correction may not be worth either the computational cost or the accumulation of numerical errors implied by the integration of this equation. We propose therefore a suboptimal approach, which consists in a different parameterization of the vector field v_u^ϕ. In Eq. (7), the momenta $\alpha_{p,j}(u)$ which parameterize v_u^ϕ are located at the positions $x_{p,\psi_1(t_j)}(u)$. One may look instead for a vector field whose momenta are located at the positions $x_{p,t_j}(u)$. In this case, Eq. (7) becomes

$$v_u^\phi(x) = \sum_{p,t_j} K^\phi(x, x_{p,t_j}(u))\alpha_{p,j}(u) \tag{15}$$

We perform the gradient descent on the same variables $\alpha_{p,j}(u)$. As a consequence, the equations (9) and (11) remain the same. In Eq. (10), $t_j(1)$ and $t'_j(1)$ must be replaced by t_j and t'_j respectively. In Eq. (12), $\tilde{A}$ is simply given by the fidelity-to-data term A (since then the regularity

term $\mathrm{Reg}\phi$ does not depend on the temporal parameters β anymore). Therefore, the Eq. (14) does not need to be implemented.

Although this solution is not optimal, the following numerical experiments tend to prove the relevance of this approximation.

4 Spatiotemporal Atlas Construction

We assume now that we have a set of N subjects (S^i), provided each with temporal observations $(S^i(t^i_j))_j$. We are looking for a template M_0 and a mean scenario of evolution of this template $M(t) = \chi_t(M_0)$, such that the observations correspond to particular moments of a spatiotemporal deformation of the mean scenario. This means that $\phi^i(M(\psi^i(t^i_j)))$ match $S^i(t^i_j)$ for each subject i and time t^i_j. Maximum A Posteriori estimation in the same setting as in [12], leads to the minimization of $J(\psi^i, \phi^i, \chi, M_0) =$

$$\sum_{i=1}^{N} \left\{ \sum_{t^i_j} \mathrm{d}(\phi^i(\chi_{\psi^i(t^i_j)} M_0), S^i(t^i_j))^2 + \gamma^{\phi}\mathrm{Reg}(\phi^i) + \gamma^{\psi}\mathrm{Reg}(\psi^i) + \gamma^{\chi}\mathrm{Reg}(\chi) \right\}$$

We perform a 3 steps alternated minimization. If the template M_0 and the regression χ are fixed, the minimum is achieved for N registrations of the mean scenario $\chi_t(M_0)$ to each subject's set of data $S^i(t^i_j)$, as in Sec. 3. If we fix the N spatiotemporal deformations (ϕ^i, ψ^i) and the regression χ, we need to minimize $\sum_{i,j} \mathrm{d}(\Phi_{i,j}(M_0), S^i(t^i_j))^2$, where the $\Phi_{i,j} = \phi^i \circ \chi_{\psi^i(t^i_j)}$ are 3D-diffeomorphisms. This is exactly the estimation of an unbiased template in forward the setting of [12], when the deformations are given by $\Phi_{i,j}$. When the template M_0 and the N spatiotemporal deformations (ϕ^i, ψ^i) are fixed, we need to minimize $\sum_{i,j} \mathrm{d}(\phi^i(\chi_{\psi^i(t^i_j)} M_0), S^i(t^i_j))^2 + \gamma^{\chi}\mathrm{Reg}(\chi)$. This is not the regression problem stated in Sec. 2 because of the deformation ϕ^i in the matching term. To turn it into regression, we approximate the matching term $\mathrm{d}(\phi^i(\chi_{\psi^i(t^i_j)} M_0), S^i(t^i_j))$ by $\mathrm{d}(\chi_{\psi^i(t^i_j)}(M_0), (\phi^i)^{-1}(S^i(t^i_j)))$ (subject's shapes are matched back to the mean anatomy). This approximation is valid only for diffeomorphisms ϕ^i whose Jacobian is close to the identity. To initialize the minimization, we set M_0 as the mean current of the earliest data and set the diffeomorphisms χ, ϕ^i, ψ^i to identity.

Eventually, this statistical estimation depends mostly on eight parameters. The degree of smoothness of each deformation (the spatial scale at which points move consistently) is controlled by a Kernel. We choose here isotropic Gaussian kernel for which the spatial scale is determined by the standard deviation λ_χ for the regression function, λ_ψ for the morphological deformation and λ_ψ for the time change function. Three parameters control the trade-off between regularity and fidelity to data: $\gamma^{\chi}, \gamma^{\phi}, \gamma^{\psi}$. The discretization step of the time interval of interest δt is also to be set by the user. Finally, the norm on currents depends on a spatial scale λ_{W^*} below which geometrical differences between shapes are considered as noise [11].

5 Numerical Experiments

Experiments were performed on two kind of data. Experiments on 2D profiles of hominids skulls relates mostly to Sec. 2 and 3, those on 3D meshes of amygdala to Sec. 4.

Evolution of 2D Curves We have five 2D-profiles of hominids skulls which consist of six lines each (source: www.bordalierinstitute.com). Our regression framework infers a continuous evolution from the Australopithecus to the Homo sapiens sapiens which matches the intermediate stages of evolution in Fig. 1.

Then, we register the evolution {Homo habilis-Homo erectus-Homo neandertalensis} to the evolution {Homo erectus-Homo sapiens sapiens} in Fig 2. The geometrical deformation shows that during the later evolution the jaw was less prominent and the skull larger and rounder than during the earlier evolution. The time change function shows that the later evolution occurs at a speed 1.66 times faster than the earlier evolution. This value is compatible with the growth speed of the skull during these periods (See Fig. 3): between Homo erectus and sapiens the skull volume growths at $(1500 - 900)/0.7 = 860\text{cm}^3/10^6\text{years}$, whereas between Homo habilis and neandertalensis, it growths at $(1500 - 600)/1.7 = 530\text{cm}^3/10^6\text{years}$, namely 1.62 times faster.

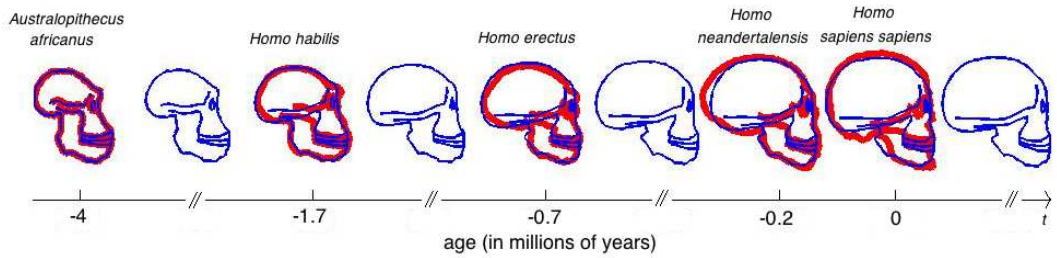

Figure 1: Skull profile of five hominids (in red). The regression model estimates a continuous evolution (in blue) of the Australopithecus, which closely matches the data.

Evolution of 3D surfaces We use here meshes of amygdala of the right hemisphere from 4 autistics, 4 developmental delay and 4 control children scanned twice [18]. Age distribution is shown in Fig 5-a. From these data registered rigidly, we infer a template, a mean scenario of evolution of this template and the spatiotemporal evolution of this mean scenario to each subject. The standard deviation of the Gaussian kernels were set to 15 mm for λ_χ and λ_ϕ and 1 year for λ_ψ; the typical scale on currents λ_{W^*} is set to 3 mm. Trade-off γ^χ, γ^ϕ were set to 10^{-3} and γ^ψ to 10^{-6}. An amygdala is typically 10 mm large. The discrete time step is set to 0.2 years.

By inspection of the companion movie, one distinguishes 4 phases during growth (See also Fig. 4). Preliminary tests do not show correlations between the morphological deformations and the pathology. From the time change functions shown in Fig. 5, we cannot conclude that a subject with pathology is systematically delayed or advanced compared to controls, even at a given age. However, the curves show that the growth speed seems to follow the same pattern, mainly an acceleration

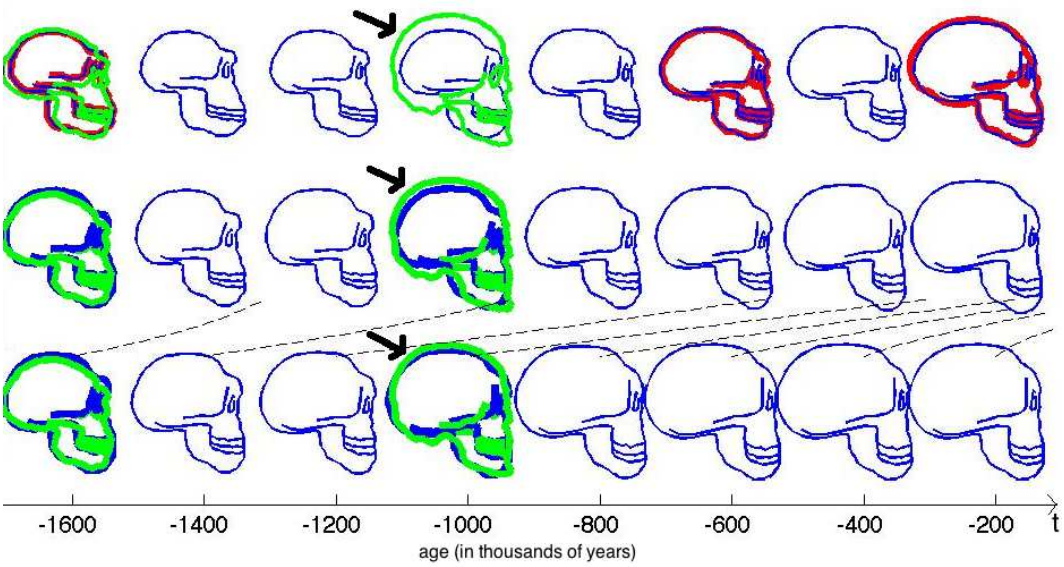

Figure 2: Registration of the evolution {Homo habilis-erectus-neandertalensis} (in red) to the evolution {Homo erectus-sapiens sapiens} (in green), shifted to start at the same time. **Top row:** Regression of the source data (red) gives the continuous evolution in blue. **Middle row:** The geometrical part ϕ is applied to each blue frame. This shows morphological changes: the skull is larger, rounder and the jaw less prominent. **Bottom row:** The time change function ψ is applied to the evolution of the second row. The blue shapes are moved along the time axis (as shown by dashed black lines), but they are not deformed. Black arrows show that a better alignment is achieved when one accounts both for morphological changes *and* a change of the evolution speed.

between age 2.5 and 3.5 for the autistics and between age 4 and age 5 for controls. The developmental delay also have such pattern but it occurs at a very variable age. These results suggest that the discriminative information between classes might not be inferred from the anatomical variability at a given age, but rather from variations of the growth process. These results, however, must be strengthen using larger database. The more time-points per subjects, the more constrained the mean scenario estimation. The more subjects, the more robust the statistics.

6 Discussion and Conclusion

In this report, we present a generic framework to analyze variability of longitudinal data. A regression model fits a continuous evolution to successive data of one subject. 4D registrations decompose the difference between two sets of longitudinal data into a geometrical deformation and a change of

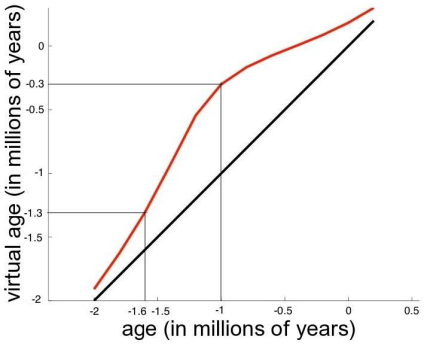

a- time change function

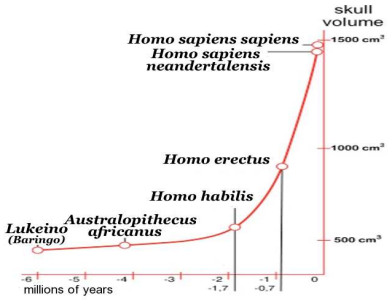

b- skull volume evolution

Figure 3: a- time change function $\psi(t)$ of the registration in Fig. 2 (in black the reference $\psi(t) = t$). The slope of the curve measures an acceleration between evolutions, which is compatible with the growth of skull volume in b (source: www.bordalierinstitute.com).

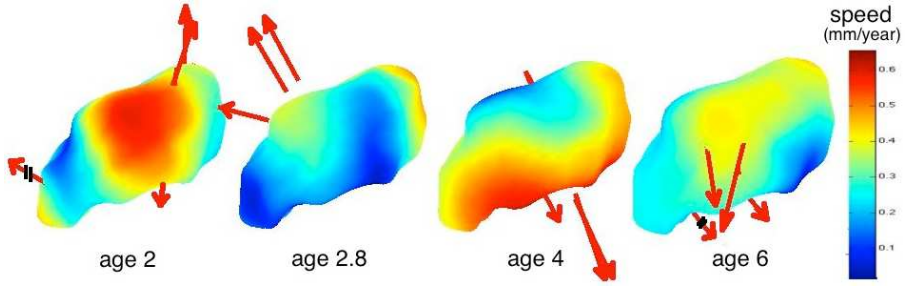

Figure 4: Mean Scenario of the right Amygdala (right lateral part). Arrows measures the differences between age t+0.2 and age t in the space of currents as in [20]. From age 2 to 2.8, the evolution is mainly a torque at the posterior part; then the structure becomes thicker, mostly at the superior part between age 2.8 and 4 and at the inferior between age 4 and 6; from age 6 the evolution is a mainly a torque at the anterior part.

the dynamics of evolution. The more acquisitions per subjects, the more constrained this decomposition. However, no constraint is imposed in terms of number and correspondence of measurement points across subjects. These pairwise registrations are used for group-wise statistics: ones estimates consistently a template, the mean evolution of this template and the spatiotemporal variability of this evolution in the population. Then, statistical measures can be derived, like the first mode of temporal deformation in Fig. 5. Further experiments have still to be performed to give more quantitative measures of variability. However, these first results suggest that pathologies might be characterized

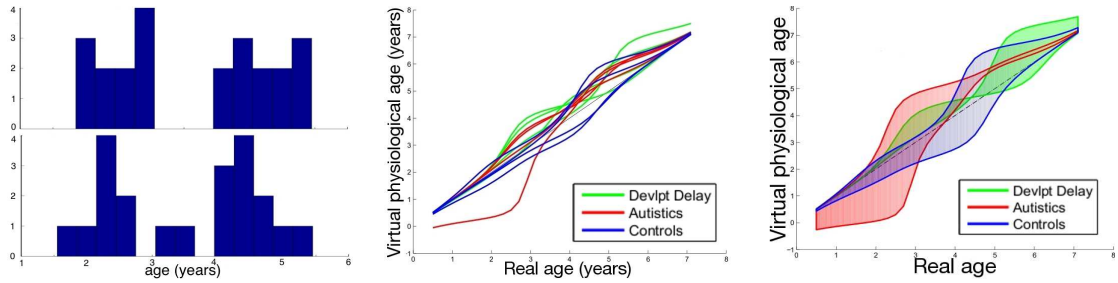

Figure 5: **Temporal deformation of the mean scenario** Left: distribution of original (top) and registered (bottom) ages. Middle: time change functions for the 12 subjects. Right: First mode of variation at $\pm\sigma$ of the time change functions for each class. Autistics and controls show the same evolution pattern, but shifted in time.

more by a particular scenario of evolution than by the anatomy at a given age. Our methodology can be used therefore to drive the search of new anatomical knowledge and to give characterization of pathologies in terms of organ growth scenario. This may be applied to the study of degenerative diseases or cardiac motion disorders.

Acknowledgments This work was partially supported the European IP project Health-e-child (IST-2004-027749) and Microsoft Research.

A Derivation of the regression criterion

In this appendix, we show how to compute the gradient of the criterion in Eq. (1). We adapt here the Large Deformation Diffeomorphic Metric Mapping (LDDMM) framework for point data [17, 13, 14] in order to take into account constraints at intermediate time-points.

M_0 is the evolving data which is made of N points x_p. The trajectories of these points are denoted: $x_p(t) = \phi_t(x_p)$. These points carry momenta $\alpha_p(t)$ which parametrize the speed vector field at each time t (See section 2). For sake of simplicity, we introduce now matrix notations: $\mathbf{x}_t$ (resp. $\boldsymbol{\alpha}_t$) denotes the $3N$ vector $(x_p(t))_{p=1\ldots N}$ (resp. $(\alpha_p(t))_{p=1\ldots N}$) and $\mathbf{k}(\mathbf{x}_t, \mathbf{x}_t)$ the $3N$-by-$3N$ matrix $K^\chi(x_p(t), x_q(t))_{p,q}$. The norm of the speed vector v_t^χ is written therefore: $\|v_t^\chi\|_V^2 = \boldsymbol{\alpha}_t^T \mathbf{k}(\mathbf{x}_t, \mathbf{x}_t)\boldsymbol{\alpha}_t$. By extension, we denote also $\mathbf{k}(x, \mathbf{x})\boldsymbol{\alpha} = \sum_i K(x, x_i)\alpha_i$. For A, a function from $\mathbb{R}^3$ to $\mathbb{R}$, we denote by $d_x A$ its Jacobian matrix at point x, so that for any vector V: $d_x A(V) = (\nabla_x A)^T V$. In turn, $\nabla_{\mathbf{x}} A$ denotes the $3N$ vector $(\nabla_{x_p} A)_p$.

With these notations, the criterion to be minimized becomes:

$$J(\boldsymbol{\alpha}) = \sum_i \mathrm{d}(\phi_{t_i}(M_0), S_i) + \gamma^\chi \int_0^T \boldsymbol{\alpha}_t^T \mathbf{k}(\mathbf{x}_t, \mathbf{x}_t)\boldsymbol{\alpha}_t dt \tag{16}$$

The fidelity term depends only on the position of the points of M_0 at the time points t_i. We write therefore this term: $A = \sum_i A_i(\mathbf{x}_{t_i})$.

We compute the variation of the criterion J with respect to a variation of the momenta: $\boldsymbol{\alpha}^\varepsilon = \boldsymbol{\alpha} + \varepsilon\tilde{\boldsymbol{\alpha}}$. These momenta yield to velocity fields v_t^ε and points trajectory $\mathbf{x}_t^\varepsilon$. We denote $\tilde{\boldsymbol{\alpha}}$ (resp. $\tilde{v}$ and $\tilde{\mathbf{x}}$) the variation with respect to ε of the momenta (resp. the velocity field and the positions): $\partial\boldsymbol{\alpha}^\varepsilon/\partial\varepsilon$ (resp. $\partial v^\varepsilon/\partial\varepsilon$ $\partial\mathbf{x}^\varepsilon/\partial\varepsilon$).

Since $v_t(x) = \mathbf{k}(x, \mathbf{x}_t)\boldsymbol{\alpha}_t$, we have :

$$\tilde{v}_t(x) = \partial_1(\mathbf{k}(x, \mathbf{x}_t)\boldsymbol{\alpha}_t)\tilde{\mathbf{x}}_t + \mathbf{k}(x, \mathbf{x}_t)\tilde{\boldsymbol{\alpha}}_t \tag{17}$$

Thanks to the flow equation (Eq. (2)), $\mathbf{x}_t = \mathbf{x} + \int_0^t v_s(\mathbf{x}_s)ds$. The variations $\tilde{\mathbf{x}}_t$ satisfy therefore:

$$\tilde{\mathbf{x}}_t = \int_0^t (\partial_1 + \partial_2)(\mathbf{k}(\mathbf{x}_s, \mathbf{x}_s)\boldsymbol{\alpha}_s)\tilde{\mathbf{x}}_s + k(\mathbf{x}_s, \mathbf{x}_s)\tilde{\boldsymbol{\alpha}}_s ds \tag{18}$$

The time-varying vectors $\mathbf{x}_t$ are solution of an inhomogeneous ordinary differential equation, which can be solved by the method of variation of parameters. Let R_{st} be the operator which gives the solution of the homogeneous equation:

$$\frac{dR_{st}}{dt} = (\partial_1 + \partial_2)(\mathbf{k}(\mathbf{x}_t, \mathbf{x}_t)\boldsymbol{\alpha}_t)R_{st} \tag{19}$$

so that the variations $\tilde{\mathbf{x}}_t$ are written as: $\tilde{\mathbf{x}}_t = \int_0^t R_{st}\mathbf{k}(\mathbf{x}_s, \mathbf{x}_s)\tilde{\boldsymbol{\alpha}}_s ds$.

We can now write the variation of the criterion J in Eq. (16) with respect to the variation $\boldsymbol{\alpha}^\varepsilon$:

$$\partial_\varepsilon J(\boldsymbol{\alpha}^\varepsilon) = \sum_i d_{\mathbf{x}_{t_i}} A_i \tilde{\mathbf{x}}_{t_i} + 2\gamma \int_0^T \tilde{\boldsymbol{\alpha}}_t^T \mathbf{k}(\mathbf{x}_t, \mathbf{x}_t)\boldsymbol{\alpha}_t dt + \gamma \int_0^T \boldsymbol{\alpha}_t^T \partial_\varepsilon(\mathbf{k}(\mathbf{x}_t^\varepsilon, \mathbf{x}_t^\varepsilon))dt \tag{20}$$

Substituting $\tilde{v}_t$ and $\tilde{\mathbf{x}}$ in this equation, the third term becomes:

$$\gamma \int_0^T \left(\int_t^T R_{ts}^T (\partial_1 + \partial_2)(\mathbf{k}(\mathbf{x}_s, \mathbf{x}_s)\boldsymbol{\alpha}_s)^T \boldsymbol{\alpha}_s ds \right)^T \mathbf{k}(\mathbf{x}_t, \mathbf{x}_t)\tilde{\boldsymbol{\alpha}}_t dt \tag{21}$$

The contribution of every A_i to first term can be written as:

$$d_{x_i} A_i(\tilde{\mathbf{x}}_{t_i}) = \int_0^T d_{\mathbf{x}_{t_i}}(A_i) R_{st_i}\mathbf{k}(\mathbf{x}_s, \mathbf{x}_s)\tilde{\boldsymbol{\alpha}}_s \mathbf{1}_{\{s \leq t_i\}} ds \tag{22}$$

where $\mathbf{1}_{\{t \leq t_i\}} = 1$ if $t \leq t_i$ and 0 otherwise (as a function of t).

The variation of the criterion is therefore:

$$\partial_\varepsilon J^\varepsilon = \int_0^T \mathbf{k}(\mathbf{x}_t, \mathbf{x}_t)(2\gamma\boldsymbol{\alpha}_t + \boldsymbol{\eta}_t)^T \tilde{\boldsymbol{\alpha}}_t dt \tag{23}$$

where $\boldsymbol{\eta}_t = \gamma \int_t^1 R_{ts}^T((\partial_1 + \partial_2)\mathbf{k}(\mathbf{x}_s, \mathbf{x}_s)\boldsymbol{\alpha}_s)^T \boldsymbol{\alpha}_s ds + \sum_i R_{tt_i}^T \nabla_{\mathbf{x}_{t_i}} A_i \mathbf{1}_{\{t \leq t_i\}}$.

The gradient of J as a L^2 function from $t \in [0,1]$ to $\mathbb{R}^{3*N}$ can now be written as: $(\nabla J)_t = \mathbf{k}(\mathbf{x}_t, \mathbf{x}_t)(2\gamma\boldsymbol{\alpha}_t + \boldsymbol{\eta}_t)$. The choice of the metric on the space of momenta (space of N L^2 functions from $[0,T]$ to $\mathbb{R}^3$) is arbitrary. For a sake of simplicity, as well as to keep closer to space induced by the velocity field, we choose $\mathbf{k}(\mathbf{x}_t, \mathbf{x}_t)$ as metric, like in [16]. Therefore, the gradient is given by:

$$(\nabla J)_t = 2\gamma\boldsymbol{\alpha}_t + \boldsymbol{\eta}_t \tag{24}$$

In order to compute the gradient, we still need to compute $\boldsymbol{\eta}_t$. For this purpose, we write the homogeneous equation (Eq. (19)) in its integral form: $R_{st} = \mathrm{Id} + \int_s^t R_{rt}(\partial_1 + \partial_2)(\mathbf{k}(\mathbf{x}_r, \mathbf{x}_r)\boldsymbol{\alpha}_r)dr$. This allows us to write $\boldsymbol{\eta}_t$ (Fubini's theorem allows us to permute two integrals, every functions being in $L^2([0,T], \mathbb{R}^{3N})$) in the form:

$$\boldsymbol{\eta}_t = \sum_i \nabla_{\mathbf{x}_{t_i}} A_i \mathbf{1}_{\{t \le t_i\}} + \int_t^T (\partial_1 + \partial_2)(\mathbf{k}(\mathbf{x}_u, \mathbf{x}_u)\boldsymbol{\alpha}_u)^T \left(\gamma\boldsymbol{\alpha}_u + \underbrace{\sum_i R_{ut_i}^T \nabla_{\mathbf{x}_{t_i}} A_i \mathbf{1}_{\{t \le t_i\}} \mathbf{1}_{\{u \le t_i\}} + \gamma \int_u^T R_{us}^T (\partial_1 + \partial_2)(\mathbf{k}(\mathbf{x}_s, \mathbf{x}_s)\boldsymbol{\alpha}_s)^T \boldsymbol{\alpha}_s ds}_{(\star)} \right) du \tag{25}$$

Now, we notice that $t \le u$ within the integral, which implies that $\mathbf{1}_{\{t \le t_i\}}\mathbf{1}_{\{u \le t_i\}} = \mathbf{1}_{\{u \le t_i\}}$. Hence, $(\star)$ is precisely equal to $\boldsymbol{\eta}_u$. Therefore, $\boldsymbol{\eta}_t$ is the solution of the integral equation (integrated upstream in time):

$$\eta_t = \sum_i \nabla_{\mathbf{x}_{t_i}} A_i \mathbf{1}_{\{t \le t_i\}} + \int_t^T \left((\partial_1 + \partial_2)\mathbf{k}(\mathbf{x}_u, \mathbf{x}_u)\boldsymbol{\alpha}_u\right)^T (\gamma\boldsymbol{\alpha}_u + \boldsymbol{\eta}_u) du \tag{26}$$

Unsurprisingly, if there is only one time point $t_1 = T = 1$, we retrieve the same gradient as for a usual pairwise 3D registrations [14, 16]. For several time-points, we solve this equation from $t = T$ to $t = 0$. The successive contributions ($\nabla_{\mathbf{x}_{t_i}} A_i \mathbf{1}_{\{t \le t_i\}}$) are added as long as t reaches 0.

The computation of $\nabla_{\mathbf{x}} A_i$ depends on the distance between data. Here we use the distance between currents. This derivation is performed as in [14, 15, 16].

References

[1] Qiu, A., Younes, L., Miller, M., Csernansky, J.: Parallel transport in diffeomorphisms distinguishes the time-dependent pattern of hippocampal surface deformation due to healthy aging and the dementia of the alzheimer's type. NeuroImage **40** (2008) 68–76

[2] Gorczowski, K., Styner, M., Jeong, J.Y., Marron, J.S., Piven, J., Hazlett, H.C., Pizer, S.M., Gerig, G.: Statistical shape analysis of multi-object complexes. Transactions on Pattern Analysis and Machine Intelligence (2009) to appear.

[3] Khan, A., Beg, M.: Representation of time-varying shapes in the large deformation diffeomorphic framework. In: Proceedings of ISBI, IEEE (May 2008) 1521–1524

[4] Davis, B., Fletcher, P., Bullitt, E., Joshi, S.: Population shape regression from random design data. In: Proc. of ICCV. (Oct. 2007) 1–7

[5] Craene, M.D., Camara, O., Bijnens, B.H., Frangi, A.F.: Large diffeomorphic FFD registration for motion and strain quantification from 3D-US sequences. In: Proc. of Functional Imaging and Modeling of the Heart. Volume 5528., LNCS (2009) 437–446

[6] Chandrashekara, R., Rao, A., Sanchez-Ortiz, G., Mohiaddin, R.H., Rueckert, D.: Construction of a statistical model for cardiac motion analysis using nonrigid image registration. In: Proceedings of Information Processing in Medical Imaging IPMI. Volume 2732 of LNCS., Springer (2003) 599–610

[7] Peyrat, J.M., Delingette, H., Sermesant, M., Pennec, X., Xu, C., Ayache, N.: Registration of 4D Time-Series of Cardiac Images with Multichannel Diffeomorphic Demons. In: Proceedings of MICCAI. Volume 5242 of LNCS., Springer (2008) 972–979

[8] Declerck, J., Feldman, J., Ayache, N.: Definition of a 4D continuous planispheric transformation for the tracking and the analysis of LV motion. Medical Image Analysis **4**(1) (1998) 1–17

[9] Perperidis, D., Mohiaddin, R.H., Rueckert, D.: Spatio-temporal free-form registration of cardiac MRI sequences. Medical Image Analysis **9**(5) (2005) 441 – 456

[10] Vaillant, M., Miller, M., Younes, L., Trouvé, A.: Statistics on diffeomorphisms via tangent space representations. NeuroImage **23** (2004) 161–169

[11] Durrleman, S., Pennec, X., Trouvé, A., Thompson, P., Ayache, N.: Inferring brain variability from diffeomorphic deformations of currents: an integrative approach. Medical Image Analysis **12**(5) (October 2008) 626–637

[12] Durrleman, S., Pennec, X., Trouvé, A., Ayache, N.: Statisticals models on sets of curves and surfaces based on currents. Medical Image Analysis (2009) To appear.

[13] Miller, M, I., Trouvé, A., Younes, L.: On the metrics and Euler-Lagrange equations of computational anatomy. Annual Review of Biomed. Eng. **4** (2002) 375–405

[14] Vaillant, M., Glaunès, J.: Surface matching via currents. In: Proc. of IPMI'05. Volume 3565 of LNCS. (2005) 381–392

[15] Glaunès, J.: Transport par difféomorphismes de points, de mesures et de courants pour la comparaison de formes et l'anatomie numérique. PhD thesis, Université Paris 13, http://cis.jhu.edu/ joan/TheseGlaunes.pdf (2005)

[16] Glaunès, J., Qiu, A., Miller, M.I., Younes, L.: Large deformation diffeomorphic metric curve mapping. International Journal of Computer Vision **80**(3) (2008) 317–336

[17] Joshi, S., Miller, M.: Landmark matching via large deformation diffeomorphisms. IEEE Transaction on Image Processing **9**(8) (2000) 1357–1370

[18] Hazlett, H., Poe, M., Gerig, G., Smith, R., Provenzale, J., Ross, A., Gilmore, J., Piven, J.: Magnetic resonance imaging and head circumference study of brain size in autism. The Archives of General Psychiatry **62** (2005) 1366–1376

[19] Durrleman, S., Pennec, X., Gerig, G., Trouvé, A., Ayache, N.: Spatiotemporal atlas estimation for developmental delay detection in longitudinal datasets. In: Proc. of MICCAI. (2009) To appear.

[20] Durrleman, S., Pennec, X., Trouvé, A., Ayache, N.: Sparse approximation of currents for statistics on curves and surfaces. In: Proc. of MICCAI'08. 390–398

Unité de recherche INRIA Sophia Antipolis
2004, route des Lucioles - BP 93 - 06902 Sophia Antipolis Cedex (France)

Unité de recherche INRIA Futurs : Parc Club Orsay Université - ZAC des Vignes
4, rue Jacques Monod - 91893 ORSAY Cedex (France)
Unité de recherche INRIA Lorraine : LORIA, Technopôle de Nancy-Brabois - Campus scientifique
615, rue du Jardin Botanique - BP 101 - 54602 Villers-lès-Nancy Cedex (France)
Unité de recherche INRIA Rennes : IRISA, Campus universitaire de Beaulieu - 35042 Rennes Cedex (France)
Unité de recherche INRIA Rhône-Alpes : 655, avenue de l'Europe - 38334 Montbonnot Saint-Ismier (France)
Unité de recherche INRIA Rocquencourt : Domaine de Voluceau - Rocquencourt - BP 105 - 78153 Le Chesnay Cedex (France)

Éditeur
INRIA - Domaine de Voluceau - Rocquencourt, BP 105 - 78153 Le Chesnay Cedex (France)
http://www.inria.fr
ISSN 0249-6399